Two charged particle and transverse energy correlations in Si+Pb collisions at 14.6A GeV/c

J. Barrette,[2] R. Bellwied,[5,*] P. Braun-Munzinger,[5] W. E. Cleland,[4] G. David,[5,†] J. Dee,[5] O. Dietzsch,[6] S. V. Greene,[7] J. R. Hall,[3,*] T. K. Hemmick,[7,‡] N. Herrmann,[5,§] B. Hong,[5] K. Jayananda,[4,‖] D. Kraus,[4] B. S. Kumar,[7] R. Lacasse,[2] D. Lissauer,[1] W. J. Llope,[5,¶] T. Ludlam,[1] R. Majka,[7] S. K. Mark,[2] S. McCorkle,[1] J. T. Mitchell,[7] M. Muthuswamy,[5] E. O'Brien,[1] C. Pruneau,[2,*] F. S. Rotondo,[7] U. Sonnadara,[4] J. Stachel,[5] E. M. Takagui,[6] H. Takai,[1] T. G. Throwe,[1] S. Voloshin,[4,**] L. Waters,[5,††] C. Winter,[7] D. Wolfe,[3] C. L. Woody,[1] N. Xu,[5] Y. Zhang,[5] Z. Zhang,[4,‡] and C. Zou[5]
(E814 Collaboration)

[1] *Brookhaven National Laboratory, Upton, New York 11973*
[2] *McGill University, Montreal, Canada*
[3] *University of New Mexico, Albuquerque, New Mexico 87131*
[4] *University of Pittsburgh, Pittsburgh, Pennsylvania 15260*
[5] *State University of New York, Stony Brook, New York 11794*
[6] *Universidade de São Paulo, São Paulo, Brazil*
[7] *Yale University, New Haven, Connecticut 06511*

(Received 15 September 1993)

We present the results of an analysis of two charged particle and transverse energy correlations in Si+Pb collisions at BNL AGS at 14.6 GeV/c per nucleon. The measured semi-inclusive normalized two-particle pseudorapidity correlation function exhibits short-range correlations similar to the correlations observed in hadron-hadron and hadron-nucleus collisions at higher energies, although the observed correlations are smaller than the values scaled from hp and hA data. Estimates, provided by the observed correlations, of the intermittency indices as well as of the parameters of the cluster model are presented. Predictions using the FRITIOF event generator, which at this level of statistical accuracy show no pseudorapidity correlations, are not in agreement with our data. Azimuthal angle two-particle correlations show nonzero back-to-back correlations in the central region (consistent with FRITIOF predictions) and are almost flat in the projectile fragmentation region. We also present results on the transverse energy azimuthal correlation function, which are similar to those from the two-particle correlation function.

PACS number(s): 13.20.Jf, 13.85.Hd

I. INTRODUCTION

In the past two decades many experiments and theoretical analyses have been performed which sought understanding of the dynamics of multiparticle production in high-energy collisions through data on inclusive distributions. However, measurements of single-particle distributions alone are insufficient to understand the details of the production mechanism. The study of correlation effects provides information on hadronic production dynamics beyond that obtained from single-particle spectra and is very important for understanding the role of resonances, minijets, strings, fireballs, etc. The correlation function, constructed in a proper way, could be a very sensitive tool for the investigation of special features of models and dynamical assumptions.

Particle correlations have been extensively studied in hadron-hadron reactions. When two-particle correlations in rapidity are studied at fixed charged particle multiplicity, apparent short-range ($\Delta y \approx 1$–2) correlations are observed [1–8]. The most successful interpretation of this correlation is found in the cluster model [9], although a physical understanding of the nature of clusters is still lacking. The study of two-dimensional correlations in rapidity and azimuthal angle space shows nontrivial azimuthal angle behavior. At ISR energies [6,7] it was

*Present address: Dept. of Physics, Wayne State University, Detroit, MI 48202.
†Present address: Brookhaven National Laboratory, Upton, NY 11973.
‡Present address: Dept. of Physics, State University of New York, Stony Brook, NY 11794.
§Present address: Physikalisches Institut, Universitat Heidelberg, D 69 Heidelberg, Germany.
‖Present address: Dept. of Physics, University of Sri Jayewardenepura, Nugegoda, Sri Lanka.
¶Present address: Dept. of Physics, Michigan State University, East Lansing, MI 48824.
**On leave from Moscow Engineering Physics Institute, Moscow, 115409, Russia.
††Present address: Los Alamos National Laboratory, Los Alamos, NM 87545.

found that the short-range rapidity correlations persist over the full azimuthal angle range, but the range of rapidity correlation is larger towards $\Delta\phi = \pi$ than towards $\Delta\phi = 0$.

The recent interest in intermittency as a probe of reaction dynamics (for a review see Refs. [10,12]) has also placed special emphasis on the study of two-particle correlations. The two-particle correlation function can be simply connected with second-order factorial moments [13,12], obtained in an intermittency analysis. Observation of intermittent behavior of factorial moments in many experiments implies the existence of short-range two-particle correlations.

The investigation of the dynamics of multiparticle production in heavy-ion collisions is particularly important because of the possibility of quark gluon plasma production in such collisions. Are there really any differences in the multiparticle production dynamics between hadron-hadron and nucleus-nucleus collisions? Do we have something new? The correlation study could be a very important part of the answer to these questions.

We present here the results of such a measurement carried out with the E814 apparatus operating at the Brookhaven AGS accelerator. Data on the inclusive charged particle multiplicity distributions [14] and transverse energy distributions [15] from this experiment have already been reported. In this paper we utilize primarily charged particle multiplicity distributions seen in 14.6 GeV/c Si-Pb central collisions to directly construct the two-particle correlation function. In our study we also explore transverse energy azimuthal angle correlations. Using transverse energy for the correlation study allows us to take into account also neutral particles and to use the data from a different detector, with totally different systematic corrections.

II. CORRELATION FUNCTION

There exist a number of different definitions of the correlation functions. In the current analysis we use one of the simplest, the normalized two-particle correlation function:

$$R(x_1, x_2) = \frac{\rho^{(2)}(x_1, x_2)}{\rho(x_1)\rho(x_2)} - 1, \tag{1}$$

where $\rho^{(2)}(x_1, x_2)$ and $\rho(x)$ are two- and one-particle densities

$$\rho^{(2)}(x_1, x_2) = \frac{1}{\sigma}\frac{d^2\sigma}{dx_1 dx_2},$$

$$\int \rho^{(2)}(x_1, x_2) dx_1\, dx_2 = N(N-1), \tag{2}$$

$$\rho(x) = \frac{1}{\sigma}\frac{d\sigma}{dx}, \tag{3}$$

and x can be any variable, such as rapidity, pseudorapidity, or azimuthal angle. The normalization of $\rho^{(2)}(x_1, x_2)$ and $\rho(x)$ is given by

$$\int \rho^{(2)}(x_1, x_2) dx_1\, dx_2 = N(N-1), \tag{4}$$

$$\int \rho(x) dx = N, \tag{5}$$

in which N is the total number of particles.

It is well known [1,2] that a mixture of events with different total multiplicities causes large positive artificial pseudocorrelations sometimes called long-range correlations. To avoid this effect one should use so-called semi-inclusive correlation functions, in which one calculates the correlation function using events with fixed total multiplicity N

$$R_N(x_1, x_2) = \frac{\rho_N^{(2)}(x_1, x_2)}{\rho_N(x_1)\rho_N(x_2)} - 1. \tag{6}$$

To avoid confusion we note here that the correlation function defined by Eq. (6) is not zero for the case of no dynamical correlation, which for this case gives $R_N(x_1, x_2) = -1/N$. This follows directly from the normalization of two- and one-particle densities [Eqs. (4) and (5)], and the fact that for the case of no correlation the two-particle density is proportional to the product of two one-particle densities. It also worthwhile to note that the function R has some scaling properties with respect to total multiplicity, or more exactly to particle density. If the correlations are mostly due to resonance decays, jet production, and analogous mechanisms, and if the relative number of these resonances or jets are the same for different multiplicities, the number of correlated pairs is proportional to N, so the peak value of R scales as $1/N$ or as $1/(dN/dy)$. For Bose-Einstein correlations the number of correlated pairs is proportional to N^2, and the correlation function in the first approximation does not depend on multiplicity.

The high statistical accuracy of our data permits a measurement of the semi-inclusive correlation function, using relatively narrow multiplicity windows. We study pseudorapidity correlations as a function of two variables and present the results for R for control bin η_1 as a function of η_2, for different total multiplicities and different azimuthal windows $\delta\phi$. For azimuthal correlations we present the results as a function of azimuthal angle difference $\Delta\phi$ between two sectors in ϕ space within a fixed pseudorapidity window $\delta\eta$.

III. EXPERIMENTAL SETUP

The E814 experimental setup, shown schematically in Fig. 1, is described in more details in Refs. [14, 15]. We use data primarily from the silicon multiplicity detector, which is complemented by data from the participant calorimeter (see the insert in Fig. 1). The multiplicity detector, shown in Fig. 2, consists of two silicon pad detectors each segmented into 512 pads. One detector, located 34 mm from the target covers the pseudorapidity region $0.87 < \eta < 1.61$, and the other, located 82 mm from the target, covers the region $1.61 < \eta < 3.86$. Pseudorapidity coverage is quoted for the case where beam particle goes through the center of the detector. The size of the

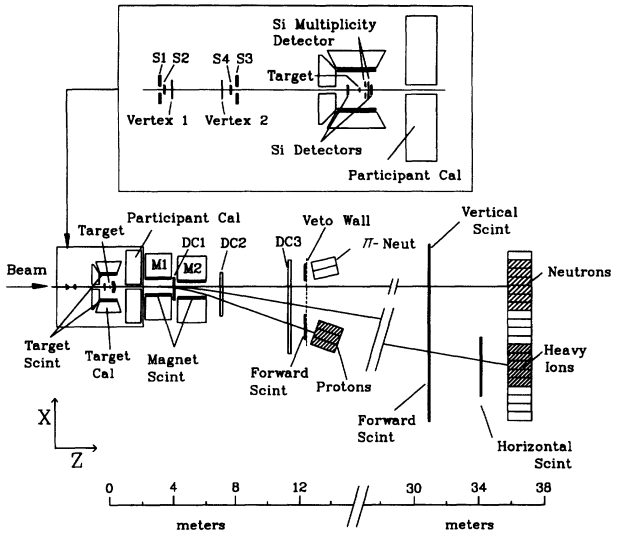

FIG. 1. Experimental setup of E814 at BNL. For this measurement, we use data from the Multiplicity Detector and the Participant Calorimeter (see insert).

pads corresponds approximately to 0.1 in both η and azimuthal angle ϕ, which determines the angular resolution in this measurement. There is no charge identification in this detector. Hits are defined by a simple threshold discriminator set to approximately 0.5 times minimum ionizing pulse height. For multiplicities around 100 the mean pad occupancy is approximately 0.1. Although the detector does not distinguish between one or more hits in the same pad, there is no need to correct for this effect for the normalized correlation function R used in the present analysis. For a determination of the autocorrelation, the effect of multiple hits could, however, be important, as is discussed below. It is also important for the multiplicity correlation analysis to take into account the exact position of the incident beam particle. The horizontal position of a beam particle is measured by a pair of silicon strip detectors, which are shown in the insert in Fig. 1, and this information is used on an event by event basis. The vertical displacement of a beam particle, caused by the beam divergence, is important mostly for the study of correlations in azimuthal angle space. The distribution of the vertical beam coordinate was assumed to be

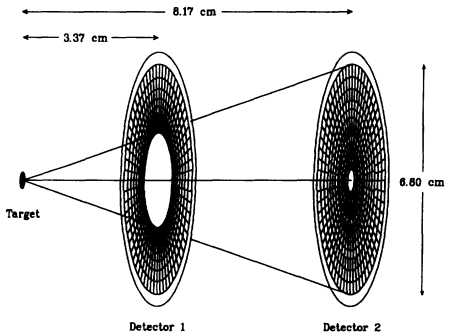

FIG. 2. E814 Multiplicity Detector ($0.8 < \eta < 3.8$).

Gaussian, and the parameters of the distribution were extracted from the multiplicity detector data (see Appendix A). The angular divergence of the beam (~ 1 mr) is much smaller than the bin widths in η and ϕ, which are set by the size of the pads.

The participant calorimeter (PCAL) is a lead-iron-scintillator sampling calorimeter. It is approximately azimuthally symmetric, built with four identical quadrants. Each quadrant of the PCAL is divided into four azimuthal slices of 22.5°. Each slice is divided radially into eight towers. This division, combined with the four depth segments, leads to a total of $32\times8 = 128$ towers for each quadrant and 512 towers for the entire calorimeter.

PCAL measures energy flow into the forward polar angle region $1.0° < \theta < 47.0°$, corresponding to pseudorapidity range $0.83 < \eta < 4.7$. It has a depth of four interactions lengths and a radius of approximately 84 cm. It is divided into two electromagnetic depth segments and two hadronic depth segments. Each of the two electromagnetic depth segments has a depth of 0.4 interaction lengths, consisting of six absorber-scintillator layers. The next 24 layers make up the first hadronic segment and the remaining 23 layers constitute the second hadronic segment. Each of the hadronic segments is approximately 1.6 interaction lengths deep.

It is also important to note that the participant calorimeter covers a pseudorapidity region similar to that of the multiplicity detector. This permits the selection of events on transverse energy deposited in the same pseudorapidity window. Data from this detector are also used for the transverse energy correlation study.

IV. ANALYSIS

A. Calculation procedure

The formula for the two-particle correlation function, describing the correlation between two bins of finite size (areas in pseudorapidity and azimuthal angle space, consisted, in our case, of one or many pads) i and k, directly follows from the definition (6):

$$R_{ik} = \frac{\langle n_i n_k \rangle}{\langle n_i \rangle \langle n_k \rangle} - 1, \tag{7}$$

$$R_{ii} = R_{\text{auto}} = \frac{\langle n_i (n_i - 1) \rangle}{\langle n_i \rangle^2} - 1, \tag{8}$$

where n_i is the multiplicity in the ith bin. The average is taken over all events with the same total multiplicity. The exact pseudorapidity, corresponding to each pad, depends on the position of the beam particle. One must be careful to correctly account for this effect. The correct formula for the correlation between two different bins is

$$R_{ik} = \frac{\langle \langle n_{i;x} n_{k;x} \rangle \rangle_x}{\langle \langle n_{i;x} \rangle \langle n_{k;x} \rangle \rangle_x} - 1, \tag{9}$$

where $\langle \rangle_x$ means average over all possible horizontal beam offsets x, and $\langle n_{i;x} \rangle$ is the mean multiplicity of the ith bin over all events with the same x beam position.

As mentioned above, there is no possibility to distinguish single from multiple hits in the same pad. This limitation becomes important for the calculation of autocorrelations, when both particles from a correlated pair occupy the same bin. The problem is easy to solve if (a) the correlation length is much larger than the size of the bin and (b) the mean pad multiplicities in the bin under study are equal to each other. In this case the fraction of all pairs which are counted as one particle is $1/l$, where l is the number of pads in the bin. Thus the correct number of pairs is the factor $(1-1/l)^{-1} = l/(l-1)$ times the observed number of pairs. In the general case this problem is circumvented by subtracting the (unknown) contribution from each single pad to the correlation function, defining the autocorrelation function to be

$$R_{\rm auto} = \frac{\langle\langle n_{i;x} n_{i;x} - \sum_j k_{ij;x} k_{ij;x}\rangle\rangle_x}{\langle\langle n_{i;x}\rangle\langle n_{i;x}\rangle - \sum_j \langle k_{ij;x}\rangle\langle k_{ij;x}\rangle\rangle_x} - 1. \quad (10)$$

Here k_{ij} is the pad occupancy (0 or 1) for the jth pad in the ith bin. By this procedure we substitute the real $R_{\rm auto}$ by the average value of all possible pad-pad correlations within the bin.

PCAL data are used for the evaluation of transverse energy correlations. The exact beam particle position is not important for these calculations due to the rather large dimensions of PCAL in comparison to the width of the beam profile, which is not the case for the multiplicity detector. We define the transverse energy correlation function as

$$R_{ik}^{E_T} = \frac{\langle E_{T;i} E_{T;k}\rangle}{\langle E_{T;i}\rangle\langle E_{T;k}\rangle} - 1. \quad (11)$$

The corresponding formula for the autocorrelation function is more complicated, because the autocorrelation depends on the form of the one-particle E_T distribution. We do not consider E_T autocorrelations in this paper.

B. Corrections and cuts

In this section we enumerate the corrections and cuts performed in the analysis. The standard event selection procedure for E814 data is described in detail elsewhere [14]. Basically, it consists of placing requirements on the beam scintillators to insure that one and only one particle of Z=14 is incident, and of a cut on the energy found in the back wall of the target calorimeter to reject events with interactions upstream of the target. The main physics trigger then requires that the total multiplicity, based on discriminator outputs, was above some minimum value.

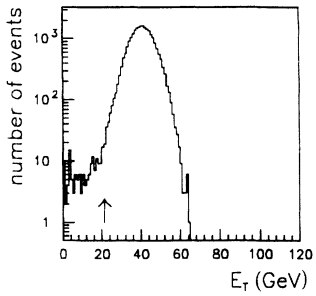

FIG. 3. Event distribution in E_T for the multiplicity window [80,100]. The required minimum value of E_T is shown by the arrow.

Due to the very high sensitivity of correlation functions to detector imperfections, the following additional selection criteria were added.

(1) Events which show very little associated transverse energy (E_T) were rejected. Our measure of transverse energy is found by performing a sum (weighted with $\sin\theta$) of the pulse heights from 512 towers of the participant calorimeter. A distribution of E_T for multiplicity triggered data is shown in Fig. 3. Events with low E_T arise from a burst of noise in the multiplicity detector in random coincidence with a beam particle, and are very effectively removed by demanding a reasonable value of transverse energy for each multiplicity window. A minimum value E_T is defined for each multiplicity window well below the peak of the distribution (see Fig. 3).

(2) Two different types of events were found to have pathological noise patterns in the hit distribution. One of these, illustrated in Fig. 4(b), occurs when noise fluctuations occur on a particular set of preamplifier channels. These events are detected by a strong cross correlation [see Fig. 4(a)] between particular channels, which permits them to be identified and removed from the sample. The second pattern, shown in Fig. 5(b), occurs due

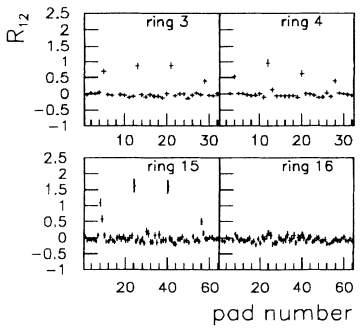

(a)

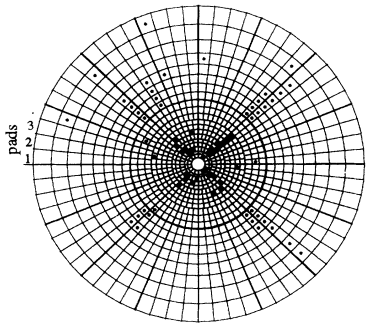

(b)

FIG. 4. (a) Correlation of the pad number 9, ring 13 with pads from rings 3, 4, 15, 16. The ring numbering starts from the most inner ring. The pad numbering starts from the horizontal plane and goes clockwise, as shown. (b) One of the "cross type" events from the multiplicity display.

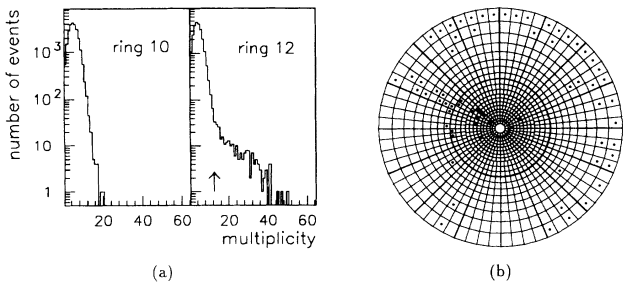

FIG. 5. (a) Multiplicity distributions in one of the inner rings (ring 10) and one of the outermost rings (ring 12). The arrow indicates the threshold used in the analysis. (b) One of the events with unusually high multiplicity in the 20th ring.

to unusually large noise fluctuation at the boundaries of the detectors. Such fluctuations result in a very high number of hits in one of the outermost rings (numbers 12 and 20). These events were removed by demanding that the multiplicities in the outermost rings be not more than some upper limit, which is determined from the ring multiplicity distributions [see Fig. 5(a)]. The definition for maximum multiplicity in these rings was analogous to the definition of minimum E_T. It was checked that both procedures if applied to the good channels (rings) do not affect the results.

The fraction of all events rejected by these two criteria is about 20%.

During the analysis of selected events some additional precautions were taken to minimize other unphysical contributions to the correlations under study.

(1) The signals from noisy pads were ignored and these pads were treated as absent, as was done in the multiplicity analysis. The total number of such pads is approximately 5%.

(2) The signals from neighboring pads in the multiplicity detector located along a radial line are processed in the same discriminator module. During the analysis it was found that there exists strong correlated noise within some discriminator modules. Therefore, for pseudorapidity correlations, we exclude contributions coming from the same discriminator module. This procedure simultaneously allows us to avoid the contribution of charge sharing to the correlation function (see below).

(3) For azimuthal correlations we exclude from the analysis the outermost rings.

(4) For the most suspicious pads the correlations with all other pads were calculated. [As an example see Fig. 4(a).] It was shown that a few pairs of pads of the detector are strongly correlated and these correlations cannot have physical origin. Such pairs were also excluded from the analysis.

There are also some other effects which could bias the results.

(1) It was found that the charge sharing between two neighboring pads could give rise to signals from both pads from a single particle. The contribution of this effect to the total multiplicity is approximately 1%, but the contribution to the correlation function could be fractionally much larger. We estimate the contribution to R to be $\Delta R_{\text{ch.sharing}} \approx 0.01/\langle n \rangle$ where $\langle n \rangle$ is mean multiplicity in the bin in question. The problem was solved by subtracting the contribution to the correlation function coming from neighboring pads in the bin under study.

(2) This procedure also avoids a second problem arising from γ conversions. As was shown in a previous analysis [16] using the FRITIOF event generator, due to the very small opening angles and the close proximity of the detector to the target, electrons from γ conversion contribute only to the same pad or adjacent pads.

(3) The corrections for the vertical beam coordinate are significant for calculations of correlations in azimuthal angle space. The corrections to the pseudorapidity correlations are rather small. The procedure used to evaluate this correction is described in the Appendix A.

V. RESULTS

A. Pseudorapidity two-particle correlations

Using the above described procedure we have calculated two particle pseudorapidity correlation functions for two different multiplicity windows and different control bins (position of η_1) as a function of η_2. The pseudorapidity correlations were calculated within fixed sectors of different size in azimuthal angle space. All data were taken with ^{28}Si projectile incident on a natural lead target, at a beam momentum of 14.6 GeV/c per nucleon. For the analysis we use multiplicity regions [80,100] and [130,150] which correspond to central collisions located on either side of the knee of the multiplicity distribution [14]. The two regions were chosen to be reasonably narrow windows of N at somewhat different centrality, both of them are located well above the trigger thresholds.

Our results for pseudorapidity correlations for multiplicity window [80,100] are presented in Fig. 6. The dashed lines in Figs. 6 and others show the value $-1/N$, which one should expect for the case of no dynamical correlation. (There is, however, a contribution from the nonzero width of the multiplicity window, which is discussed below in the comparison with a cluster model.) We see clearly the short-range pseudorapidity correlations in the data for large azimuthal angle intervals. Note that the errors in the figures (we use one standard deviation for the error bars) are calculated under the assumption that the data points are independent. Because of strong correlations introduced by the calculation procedure they do not represent the true errors for the relative difference between points. Different data points are not independent because the same data for the control bin are used to calculate the correlations with all other bins. This is why most of the points lie on the smooth curve within their errors.

The FRITIOF results for the same control bins and two multiplicity windows similar to those used for the data are presented in Fig. 7. There exist other event generators such as ARC (A Relativistic Cascade) and RQMD (Relativistic Quantum Molecular Dynamics) which in some cases describe better the data at AGS energies. Their disadvantage is that they are much slower than FRITIOF, and our studies require very high statistics.

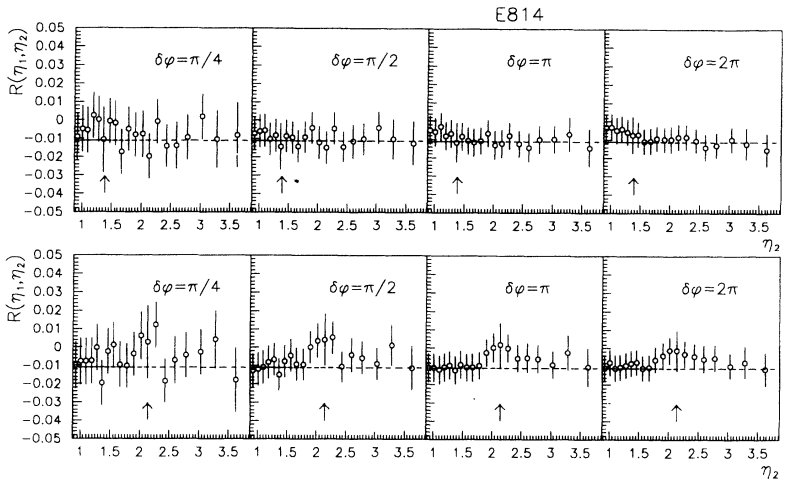

FIG. 6. The correlation function $R(\eta_1,\eta_2)$ for η_1=1.35 and 2.15, indicated by arrows on the graphs, as a function of η_2 calculated within different azimuthal angle sector sizes $\delta\phi$. Multiplicity window [80,100]. 27 000 events.

FRITIOF does contain all the main features which we believe to be important for correlation studies such as momentum and charge conservation. From the comparison of our data with scaled hadron-hadron and hadron-nucleus data (see below) it seems that the effects of intranuclear cascading (which FRITIOF does not have) are not very important for our case.

To reduce the statistical errors, we average the correlation function over a small pseudorapidity region, assuming that the correlation function $R(\eta_1,\eta_2)$ for a variation of η_1 within a small region $\delta\eta$ depends only on the difference $(\eta_1-\eta_2)$. We calculate the correlation function for different control bins (η_1) in this region (we use regions containing three bins), and, assuming translation invariance of the correlation function, average it over the region. Note that we do not lose resolution by this procedure; it is not equivalent to increasing the size of the pseudorapidity bins. The results of such averaging are presented in Fig. 8 (multiplicity window [80,100]) and in Fig. 9 ([130,150]). To see the effect one should compare Fig. 8 with corresponding graphs of Fig. 6. For each graph with $\eta_1=1.75$, which is rather close to the boundary of both detectors, the data adjacent to the boundary are omitted, as they are strongly biased by the overlapping of the two detectors.

For higher multiplicity, the correlations are smaller, as expected from $1/N$ scaling. The height of the correlation function appears to increase with decreasing size of the azimuthal angle sector; for the smallest sector it is approximately twice as large as the value found for the whole ring.

In contrast to the real data, the data from the FRITIOF event generator, which are presented in Fig. 10 (pseudorapidity correlations within a whole ring in the azimuthal angle space, $\delta\phi=2\pi$) show no pseudorapidity correlation at the same level of accuracy (a few tenths of a percent). The FRITIOF results for other multiplicity windows are similar.

Due to the scaling properties of the normalized two-particle correlation function it is possible to make a comparison with the data from hadron-hadron and hadron-nucleus interactions at higher energies [3–7]. For example, in meson-nucleus (K^+,π^+)+(Al,Au) NA22 data [3], the peak value of the two charged particle correlation function $R(0,0)$ is close to 0.3, for $dN/d\eta\approx 2.6$. This results in $R\approx 0.015$ when scaled to our particle density $dN/d\eta(\eta=1.3)\approx 50$ (multiplicity window [80,100]), All other sets of data, when scaled to our multiplicity densities, give for the peak correlation function values from 0.01 to 0.03.

Split-bin correlation functions [18] (SBCF) have been used by Seibert [19] to analyze the data [20] from O+Em and S+Em collisions at 200 GeV/nucleon. The SBCF is very close to the second-order factorial moment and two-particle correlation function [very roughly $S_2(\delta y)\approx R(\delta y/2)$], but has some important advantages such as the use of independent data for the calculation in different rapidity intervals and the possibility to extend correlation calculations to other quantities (such as transverse energy) in a natural way. Moreover, although the semi-inclusive correlations are not studied in Ref. [19], an event-by-event multiplicity correction and a correction for the shape of single-particle density are introduced. The function $\langle N/\Delta Y(S_2-\tilde{S}_2)\rangle$ is constructed, where N

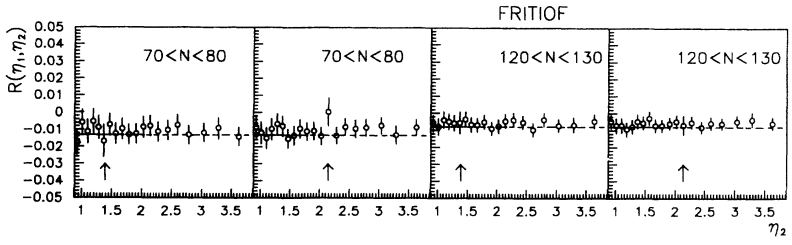

FIG. 7. The correlation function $R(\eta_1,\eta_2)$ for $\eta_1=1.35$ and 2.15, indicated by arrows on the graphs, as a function of η_2 calculated within azimuthal angle sector sizes $\delta\phi=2\pi$.

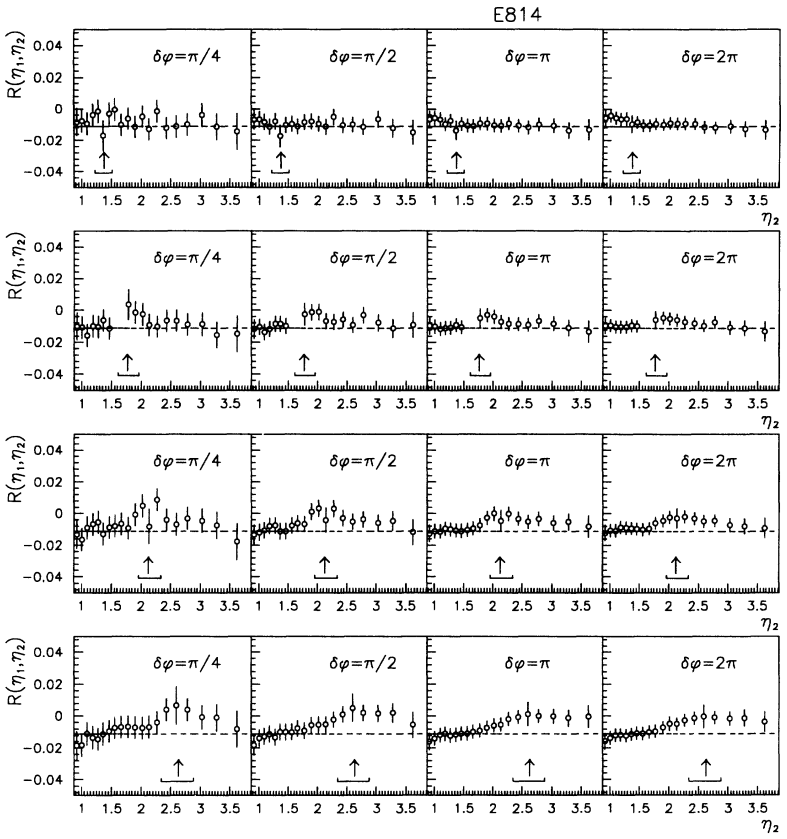

FIG. 8. The same as Fig. 6 after averaging of the correlation function $R(\eta_1, \eta_2)$ within small region of η_1 shown in the figure by square brackets. Positions of the control bin $\eta_1 = 1.35$, 1.75, 2.15, and 2.55 are indicated by arrows.

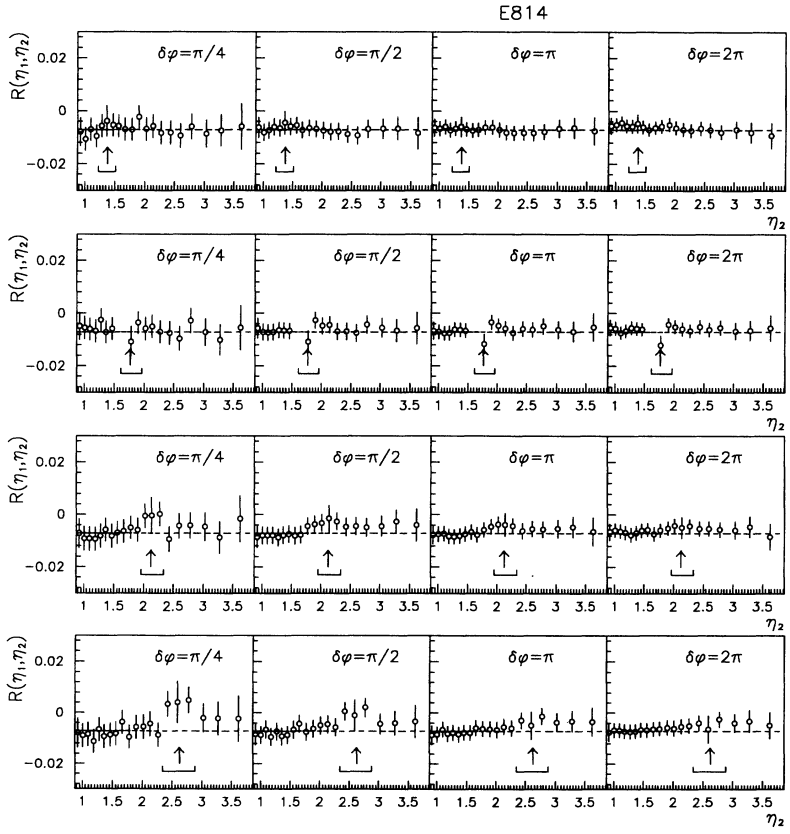

FIG. 9. The same as Fig. 8 for multiplicity window [130,150]. 55 000 events.

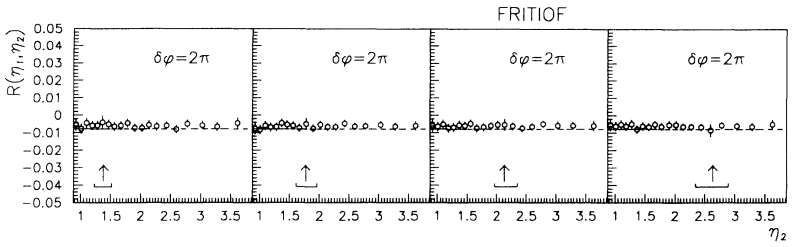

FIG. 10. FRITIOF predictions for correlation function $R(\eta_1, \eta_2)$ for $\eta_1 = 1.3$ and 2.15 indicated by arrows on the graphs, as a function of η_2. Multiplicity window [120,130].

is the total multiplicity, ΔY is total rapidity region, S_2 is the SBCF, and $\tilde{S}_2$ is the value of the correlation function in the absence of dynamical correlations [19] (due to the shape of the single-particle density distribution). For comparison we note that the height of our correlation function (~ 0.01) multiplied by the typical single-particle densities ($dN/d\eta \sim 50$–80) yields values comparable to those found by Seibert, although we cannot support his conclusion that the observed correlations in AA collisions are strongly enhanced compared to values observed in e^+e^- or πp collisions. In fact, as discussed above, our observed correlations are somewhat smaller than what expected from hadron-hadron data taken at higher energies. The somewhat stronger correlations seen by Seibert could result from higher energy used in the emulsion experiment (see discussion in the Sec. V A 1).

For a more accurate comparison of our data with the data from other experiments we fit the correlation functions using a simple cluster model and using the form of two-particle density which leads naturally to "intermittent" behavior of the scaled factorial moments. In the Fig. 11 we present for illustrative purposes the results of the fit to the data for multiplicity window [80,100] for the control bins $\eta_1 = 2.15$ and $\eta_1 = 2.55$, and $\delta\phi = 2\pi$.

1. A cluster model

In this model [9,4] two-particle correlations are due to the production of clusters (which could be the usual resonances) and their decays. The main ideas behind this model are discussed in Appendix B. The expression we used to fit our data, is

$$R(\eta_1,\eta_2) = \beta \cdot \frac{\rho[(\eta_1+\eta_2)/2]}{\rho(\eta_1)\rho(\eta_2)} \frac{1}{2\sqrt{\pi}\delta} \exp\left(-\frac{(\eta_1-\eta_2)^2}{4\delta^2}\right) - (1+\beta)\frac{1}{\langle N\rangle} + \frac{\langle N^2\rangle - \langle N\rangle^2}{\langle N\rangle^2}, \quad (12)$$

where δ and β are parameters, and $\rho(\eta)$ is the single-particle density. In the cluster model $\beta = [\langle k(k-1)\rangle/\langle k\rangle]|_N$, where k is the multiplicity of charged particles in the cluster. The last term in Eq. (12) represents the contribution to the normalized correlation function R from the nonzero width of the multiplicity window. It is the value of the correlation function (9) under the assumptions of (a) no dynamical correlation and (b) the proportionality of particle rapidity density within the selected multiplicity window to the total multiplicity.

The same formula is also used for fitting the pseudorapidity correlation within azimuthal angle sectors of different sizes. Strictly, Eq. (12) is valid for correlations over all ϕ. For correlations in an azimuthal sector of width $\delta\phi$, in principle it is necessary to modify the first term by the probability of finding both particles in the same sector and to divide by the product of the single-particle densities in ϕ. For the case of very weak azimuthal correlations the ratio is close to 1, and can therefore be ignored. Unfortunately, statistical errors do not allow us to extract all parameters with good accuracy. The mean value for δ is close to 0.4. Qualitatively we observe that the width δ increases slightly as $\delta\phi$ increases. In the Table I we present the fitted values for the parameter β extracted under the assumption of $\delta = 0.35$ and $\delta = 0.45$, for different ϕ sector sizes. The errors in the table were obtained in the following way. As mentioned above, the points for the correlation function $R(\eta_1, \eta_2)$ for fixed η_1 as a function of η_2 are positively correlated due to the use of the same data for the control bin, which has effect of reducing the fluctuations between different points. It is nontrivial to calculate the exact covariance matrix, so we use the following simpler procedure. The errors were calculated under the assumption that there were no correlation between points, and the χ^2 per degree of freedom was rescaled to 1, giving scaled values for errors.

The extracted β and δ parameters are both somewhat smaller than those obtained from an analysis of hadron-hadron data at higher energies. ISR and Collider data [6,4] igive values for β of 1.2 ± 0.2 and 1.45 ± 0.15, respectively, and for the δ parameter values in the range 0.6–0.8 depending on total multiplicity. Our smaller β value could be qualitatively explained by the fact that our energy is much lower, so the average cluster size should be smaller. The smaller value of the width δ could also originate in the lower energy. At AGS energies the most frequently produced resonance is $\Delta(1232)$, which decay

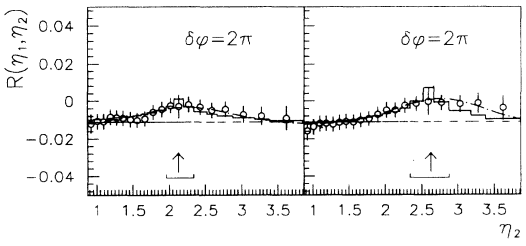

FIG. 11. The results from Fig. 8 for the control bins $\eta_1 = 2,15$ and 2.55 and $\delta\phi = 2\pi$ in comparison with fits using cluster model (smooth curve) and "intermittent" form of two particle density (histogram).

TABLE I. Parameter $\beta = \langle k(k-1)\rangle/\langle k\rangle$ for different values of width δ and sector sizes $\delta\phi$. Errors shown after rescaling χ^2 (see text). Multiplicity window [80,100].

Width	Sector size	Control bin η_1			
δ	$\delta\phi$	1.27	1.87	2.14	2.59
0.35	$\pi/4$	0.23±0.14	0.49±0.11	0.60±0.14	0.54±0.06
	$\pi/2$	0.16±0.11	0.40±0.10	0.54±0.10	0.51±0.04
	π	0.30±0.10	0.36±0.10	0.44±0.07	0.46±0.04
	2π	0.34±0.06	0.36±0.07	0.38±0.04	0.44±0.04
0.45	$\pi/4$	0.27±0.16	0.76±0.15	0.85±0.21	0.71±0.12
	$\pi/2$	0.30±0.13	0.58±0.15	0.75±0.14	0.67±0.04
	π	0.45±0.12	0.56±0.11	0.65±0.11	0.60±0.04
	2π	0.36±0.06	0.56±0.07	0.56±0.06	0.56±0.03

to nucleon and pion with relatively small momentum in the resonance system. The maximum rapidity separation between nucleon and pion is ≈ 1.2. After fitting with a Gaussian, the width is significantly smaller than for most other resonances. The fact that we do not locate our control bins in the center of the rapidity distribution, as was done for the ISR and Collider energies, could also slightly influence the results.

The two-dimensional correlation analysis of the ISR data [6] shows broader pseudorapidity correlations for the particles located back-to-back in the azimuthal space.

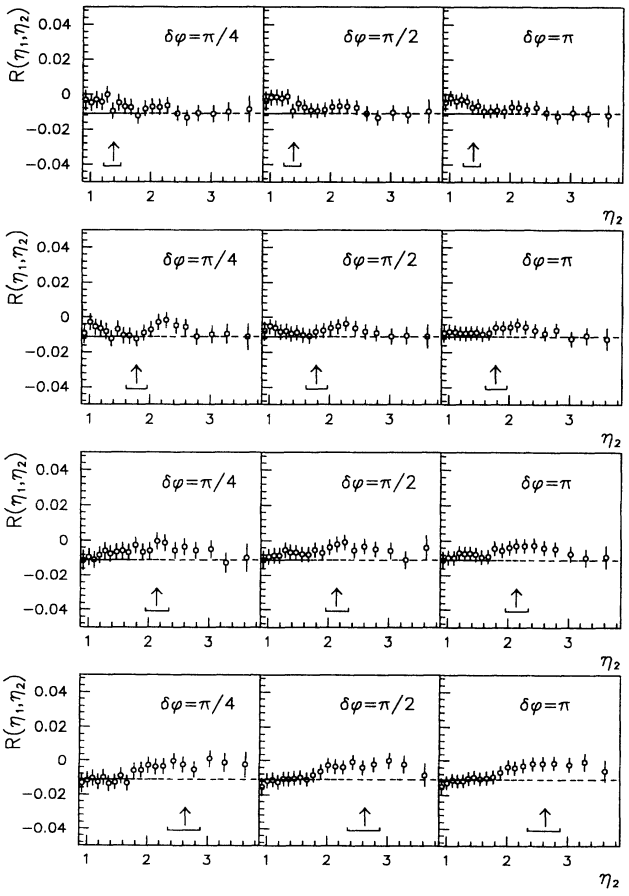

FIG. 12. The same as Fig. 8 for correlations between opposite sectors.

With the same cluster model parameters they obtain $\delta \approx 0.5$ for particles separated in azimuthal space by $\Delta\phi < \pi/2$ and $\delta \approx 0.9$ for $\Delta\phi > \pi/2$. Qualitatively this result is consistent with our data, which give a smaller value of δ for small $\delta\phi$. We can see the analogous effect by calculating the pseudorapidity correlations between particles produced in the sectors located opposite to each other. In Fig. 12 the results of such an analysis are presented for different sector sizes and different values of η_1. If we fit these data by the same formula, we get values of δ larger by about 0.1.

2. *Intermittency*

Although there are at present no semi-inclusive measurements of the factorial moments, it is very interesting to compare our results with factorial moments data, because of the intimate connection between two-particle correlation function and the second-order factorial moment. A simple relation between those two quantities can be derived under the assumption that one-particle density does not depend on rapidity [$\rho^{(1)}(y)$=const=a] and a two-particle density function depends only on the difference between y_1 and y_2:

$$\rho^{(2)}(y_1, y_2) = \rho^{(2)}(y_1 - y_2) = \rho^{(2)}(y_2 - y_1).$$

Using the definition of the second-order factorial moment one gets

$$F_2(\Delta y) = \frac{\int_0^{\Delta y} dy_1 \int_0^{\Delta y} dy_2 \rho^{(2)}(y_1, y_2)}{\left[\int_0^{\Delta y} dy_1 \rho^{(1)}(y_1)\right]^2} = \frac{2\int_0^{\Delta y} dy_1 \int_0^{y_1} dy_2 \rho^{(2)}(y_1 - y_2)}{(a\Delta y)^2}. \quad (13)$$

Multiplying through by $(a\Delta y)^2$ and taking the second derivative with respect to Δy we immediately have

$$[(a\Delta y)^2 F_2(\Delta y)]'' = 2\rho^{(2)}(\Delta y). \quad (14)$$

If, as was found in many experiments, the factorial moments exhibit intermittent behavior, i.e.,

$$F_2 = c(\Delta y)^{-\phi_2}, \quad (15)$$

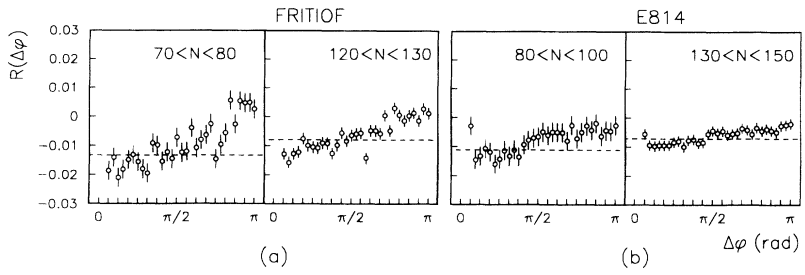

FIG. 13. The correlation function $R(\Delta\phi)$ as a function of azimuthal angle difference $\Delta\phi$ between two bins of azimuthal angle size $\pi/32$ and pseudorapidity $0.96 < \eta < 1.61$ for FRITIOF and Si+Pb data. Multiplicity windows are shown in the graphs.

then the two-particle density should follow the same power law:

$$\rho^{(2)}(\Delta y) = \frac{ca^2}{2}(2-\phi_2)(1-\phi_2)(\Delta y)^{-\phi_2}. \tag{16}$$

The experimental nucleus-emulsion data on the second-order (inclusive) factorial moment give for the intermittency indices ϕ_2 values from 0.002 to 0.008 for our particle densities (see the compilation in Adamovich *et al.* [17]). For example, a value $\phi_2 = 0.005$ implies that for Δy values of 0.2 and 1.0 the two-particle density differs by a factor 1.008 and the two-particle correlation function, which is directly related to $\rho^{(2)}$, changes by 0.008. This value is somewhat larger than could be expected from our data. Our data can be fitted, by directly using Eq. (16), taking into account the finite bin width. In this case for the pseudorapidity correlation between bins $[a_1, b_1]$ and $[a_2, b_2]$ we have:

$$R_{12} = \frac{\int_{a_1}^{b_1} d\eta_1 \int_{a_2}^{b_2} d\eta_2 \rho^{(2)}(\eta_1, \eta_2)}{\int_{a_1}^{b_1} d\eta_1 \rho^{(1)}(\eta_1) \int_{a_2}^{b_2} d\eta_2 \rho^{(1)}(\eta_2)} - 1. \tag{17}$$

A fit to our data gives intermittency indices, for different control bins, from 0.001 to 0.005 for the multiplicity window [80, 100] and less than 0.002 for the multiplicity window [130,150]. Although these values were obtained under a very crude approximation, we conclude that our data do not contradict the intermittency data; however, more precise measurements are needed for a stronger conclusion.

B. Azimuthal correlations

In this section we discuss azimuthal multiplicity and transverse energy correlations for different pseudorapidity regions. The corrections for the vertical beam position distribution are significant here for multiplicity correlations, but the systematic errors arising from this correction are much smaller than the statistical errors shown in the figures, due to the rather good accuracy of the extracted parameters of the beam vertical position distribution (see Appendix A).

The multiplicity correlation functions in the azimuthal angle space, calculated within pseudorapidity window [0.96,1.61] [see Fig. 13(b)] show nonzero back-to-back correlations. These results are consistent with FRITIOF calculations [Fig. 13(a)] and the ISR pp results [6]. This feature is very probably the consequence of the global momentum conservation, which should be very important for a large pseudorapidity region. It could also be the consequence of a nonzero impact parameter. This latter very interesting possibility needs more extensive study.

The azimuthal correlations for smaller pseudorapidity regions depend on the location of the pseudorapidity interval (see Fig. 14). Pseudorapidity windows located in the central region give back-to-back correlations, but windows in the projectile fragmentation region result in

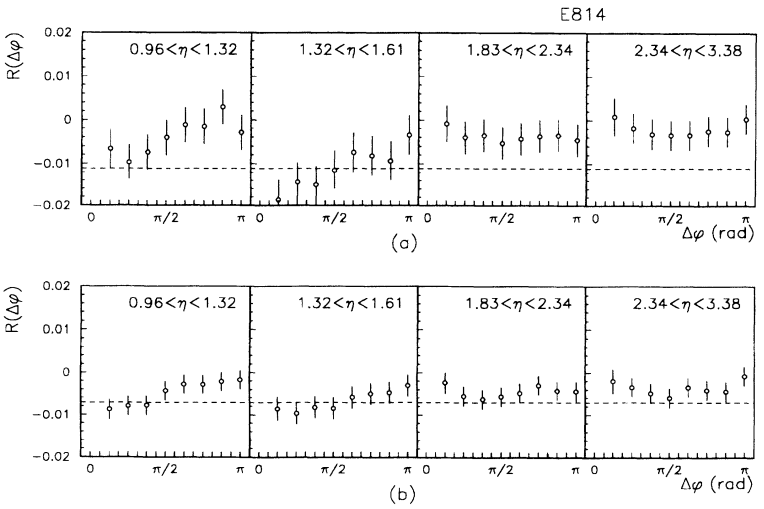

FIG. 14. The correlation function $R(\Delta\phi)$ as a function of azimuthal angle difference $\Delta\phi$ between two bins of azimuthal angle size $\pi/8$ for different pseudorapidity regions. (a) Multiplicity window [80,100]. (b) Multiplicity window [130,150].

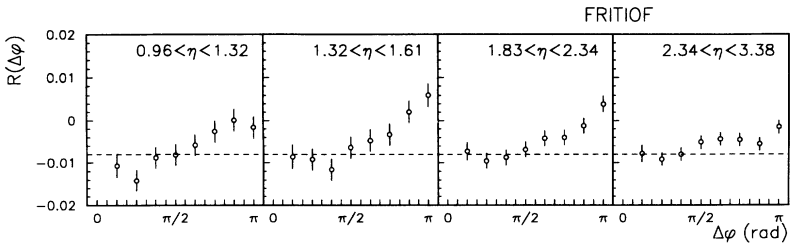

FIG. 15. FRITOF predictions for the correlation function $R(\Delta\phi)$ as a function of azimuthal angle difference $\Delta\phi$ between two bins of azimuthal angle size $\pi/8$ for different pseudorapidity regions. Multiplicity window [120,130].

positive (relative to $-1/N$) correlations. FRITIOF predicts a much smaller difference in back-to-back correlations between different pseudorapidity intervals (Fig. 15).

In contrast to the azimuthal multiplicity correlations the azimuthal transverse energy correlations do not require any corrections for the vertical beam position. The participant calorimeter, as mentioned above, consists of the 16 ϕ-symmetric sectors, so we have the same sector size as for multiplicity analysis. The (raw) transverse energy distribution for multiplicity window [80,100] and the total measured pseudorapidity range is shown in Fig. 3. Although the distribution is rather narrow, a mixture of events with different E_T causes positive pseudocorrelation, just as a mixture of events with different multiplicities does for the multiplicity correlations. Therefore, in Fig. 16 we show the results for different relatively small transverse energy regions. In this figure we present results for events with total multiplicity from the regions [80,100] and [130,150].

We can estimate the value of the pseudocorrelation due to the nonzero width of the transverse energy window, under the assumption of proportionality of the transverse energy pseudorapidity distribution to the total transverse energy (within a narrow multiplicity window or almost constant centrality). In this case $\Delta R^{\text{pseudo}} = \langle \Delta E_T^2 \rangle / \langle E_T \rangle^2$. These quantities have been calculated along with the correlation functions and are presented in Table II. The value of the correlation function at $\pi/2$ is also given for comparison. One can see that this effect explains most but not all of the difference between correlation functions using all E_T events and narrow windows. We suspect that the residual effect is due to a difference in the shape of the transverse energy pseudorapidity distribution for different total E_T. The changes in the mean multiplicities corresponding to the different E_T regions are negligible (see Table II).

The E_T azimuthal correlations show a behavior analogous to the multiplicity correlations. In Fig. 17 we present also transverse energy azimuthal correlations for different pseudorapidity regions (compare to Fig. 14). To compare E_T correlations with multiplicity correlations one should consider that E_T correlations take into account the contribution from neutral particles. We also cannot avoid without complicated corrections the effects of shower spreading, which cause large positive correlations within the size of the shower. For large pseudorapidities this effect, unfortunately, could be dominant. To be less sensitive to shower spreading in current analysis we used transverse energy produced in the two electromagnetic sections and only the first hadronic section of the calorimeter, but the effect can still be significant.

VI. DISCUSSION AND CONCLUSION

We have presented the results of a two-particle and transverse energy correlation analysis of the Si+Pb collision data at AGS energies. The use of relatively small multiplicity windows allows us to avoid pseudocorrelations from mixing of the events with different total multiplicities. We see the short-range correlations, simi-

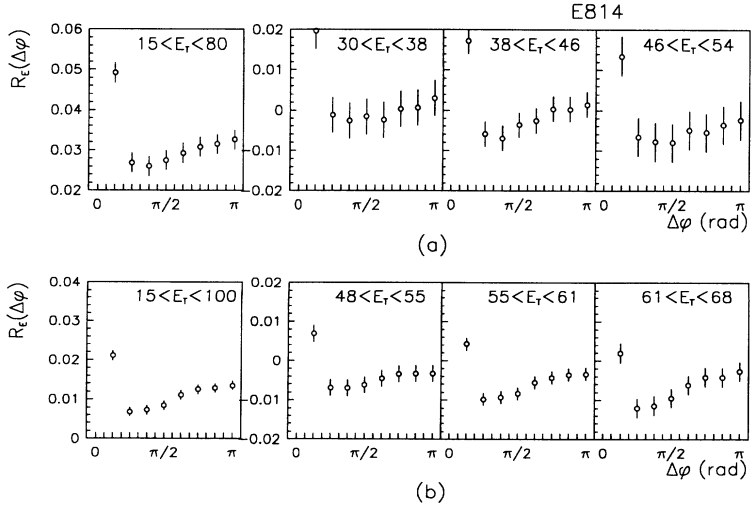

FIG. 16. Transverse energy correlation function $R_E(\Delta\phi)$ as a function of azimuthal angle difference $\Delta\phi$ between two bins of azimuthal angle size $\pi/8$ and pseudorapidity $0.96 < \eta < 1.61$ for different E_T regions (shown in GeV). (a) Multiplicity window [80,100]; (b) Multiplicity window [130,150].

TABLE II. ΔR^{pseudo} for different multiplicity windows and E_T cuts.

Multiplicity window	E_T window (GeV)	$\langle \Delta E_T^2 \rangle / \langle E_T \rangle^2$	$R_E(\pi/2)$	$\langle N \rangle$
[80,100]	All	0.023	0.027	89.6
	[30,38]	0.004	-0.002	87.1
	[38,46]	0.003	-0.004	89.9
	[46,54]	0.002	-0.008	92.9
[130,150]	All	0.0081	0.008	138.4
	[48,55]	0.0012	-0.006	137.5
	[55,61]	0.0009	-0.009	138.6
	[61,68]	0.0008	-0.010	139.6

lar to the well-known correlations observed in hadron-hadron and hadron-nuclei collisions at higher energies. The heights of the normalized correlation functions are somewhat smaller than values obtained by $1/N$ scaling of the hp and hA data. Analysis of our data within a simple cluster model gives results comparable to those found at Fermi National Accelerator Laboratory, and ISR and Sp$\bar{p}$S colliders at CERN. However, our data favor somewhat smaller values for the width of the cluster decay distribution and mean multiplicity of cluster decay than the higher energy data. A qualitative explanation for the difference may lie in the fact that present experiment is done at lower energy and does not produce heavy resonances with large probability.

There exist no AA data on two-particle correlations with which to make comparisons. We have attempted to extract relevant information from AA factorial moment data. Because of the intimate connection between the two-particle correlation function and the scaled second-order factorial moment, one should be able to directly relate the latter to our measurements. However, all the available data are for inclusive factorial moments only, and we were unable to take into account in a sufficiently reliable way the mixture of events with different multiplicities. The analysis of our data under the assumption of intermittent type behavior of the two-particle correlation function gives intermittency indices for different pseudorapidity regions from 0.001 to 0.005 for multiplicity window [80,100] and less than 0.002 for multiplicities [130,150].

The FRITIOF event generator, which shows at this level of accuracy (a few tenths of a percent for the normalized correlation function), no pseudorapidity correlations, does not agree with our results. Although the FRITIOF results always underpredicts semi-inclusive two-particle correlations, the difference for AA collisions is larger. As for azimuthal two-particle correlations the agreement between FRITIOF and the data is better, although in the projectile fragmentation region the data exhibits no back-to-back correlations while the FRITIOF data does predict such an effect. For relatively large pseudorapidity windows the clearly evident back-to-back correlations are most likely due to momentum conservation but could be also due to nonzero impact parameter collisions. In the fragmentation region, diffraction could play an essential role, and the study of correlations in this region could provide us important information on the propagation of diffractively excited hadrons through nuclear matter.

Our results are consistent with that observed in the SBCF analysis of O+Em and S+Em collisions at 200 GeV/nucleon. The slightly larger correlations seen in the emulsion experiment can be explained by the difference in beam energy for the two different experiments.

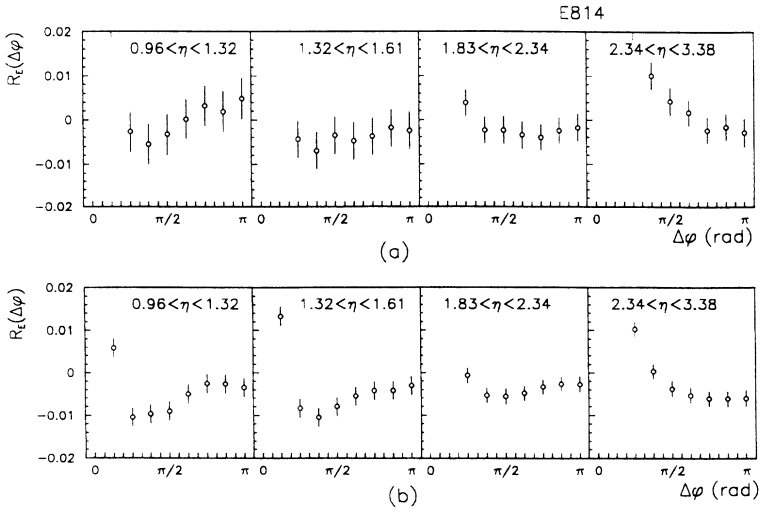

FIG. 17. Transverse energy azimuthal correlations for different pseudorapidity regions. (a) Multiplicity window [80,100], 38 GeV$< E_T <$ 46 GeV. (b) Multiplicity window [130,150], 55 GeV $< E_T <$ 61 GeV.

For the first time we present a measurement of the transverse energy correlation function. Although these correlations are distorted at small $\Delta\phi$ or $\Delta\eta$ by the shower spreading in the calorimeter, they have some clear advantages. They are insensitive to the effects of low-energy charged particles and δ rays, and, in this experiment, there is no need to make corrections for the beam position variations, due to the large size of the calorimeter. The E_T correlations give us the possibility to take into account also neutral particles and study the correlations between all produced particles, which can be important in some investigations.

Our results do not indicate any "new" physics of multiparticle production in the AA collisions at AGS energies. However, the study of AA collisions with its high multiplicities and statistics permits a study of semi-inclusive two-particle correlations with good accuracy in a relatively wide range of pseudorapidity. The two-particle correlations in hh collisions are strongly affected by different conservation laws: conservation of the momentum, charge, and baryon number. The correlations in AA collisions could be less sensitive to these effects.

ACKNOWLEDGMENTS

This research was supported, in part, by the U.S. DOE under Contract No. DEAC02-CH00016, the NSF, and Natural Sciences and Engineering Research Council of Canada.

APPENDIX A: CORRECTIONS FOR THE VERTICAL BEAM POSITION DISTRIBUTION

In the present experiment the vertical position was not measured on an event by event basis. But fortunately, knowledge of $dn/d\eta$, measured in the same experiment, and of the distribution of the vertical beam offset, which is measured in the multiplicity detector, allow one to calculate the corrections analytically without needing to know the exact beam position in each event. The correction procedure for the normalized two-particle correlation function due to the vertical beam position distribution can be described by the formula:

$$R_{ik}^{\text{corrected}} = (R_{ik}^{\text{uncorrected}} + 1)/K_{ik} - 1, \tag{A1}$$

where the correction coefficient K_{ik} is

$$K_{ik} = I_{ik}/I_i \cdot I_k, \tag{A2}$$

$$I_{ik} = \int dy\, P(y) \int_{\Delta\eta_i\delta\phi_i} d\eta_i d\phi_i \times \int_{\Delta\eta_k\delta\phi_k} d\eta_k d\phi_k \frac{d^2n}{d\eta_i d\phi_i}(\eta_i, \phi_i; y) \times \frac{d^2n}{d\eta_k d\phi_k}(\eta_k, \phi_k; y), \tag{A3}$$

$$I_j = \int dy P(y) \int_{\Delta\eta_j\delta\phi_j} d\eta_j d\phi_j \frac{d^2n}{d\eta_j d\phi_j}(\eta_j, \phi_j; y). \tag{A4}$$

Here pseudorapidity η and azimuthal angle ϕ are calculated in the coordinate system centered on the detector. $P(y)$ is the normalized vertical distribution of the beam particle at the target.

As mentioned above, it was assumed that the distribution $P(y)$ is Gaussian. The width of the distribution was determined by measuring the spatial distribution of coincidences between selected cells in each plane of the multiplicity detector. The distribution of such coincidences is quite sensitive to the distribution of beam particles. It is due to a small overlap of the two detectors at off axis beam particles (see Fig. 18). We choose as a control pad one of the pads located in the horizontal plane from the innermost ring of the first detector. We used pads in the horizontal plane due to nonzero horizontal mean offset (measured by the vertex silicon strip detector). We then study the coincidence of hits in this pad with six pads from the second detector. We take three pads from each of two outermost rings of the second detector. To extract the parameters of beam position distribution we minimize the function:

$$\chi^2(y_0, \sigma_y) = \sum_i \frac{(N_i - N_i^{\text{est}})^2}{N_i} \tag{A5}$$

with respect to the parameters of the distribution centroid y_0 and variance σ_y. In Eq. (A5) N_i is the number of hits in the ith pad under the condition that there is a hit in the control pad. N_i^{est} is estimated number of hits using the assumed distribution for vertical beam position.

To calculate N_i^{est} we use the formula:

$$N_i^{\text{est}} = \int dx \frac{dN_{\text{cntr}}}{dx} \int dy\, P(y; y_0, \sigma_y) \times \{1 - \exp[-\tilde{n}_i^*(x, y)]\}, \tag{A6}$$

where $dN_{\text{cntr}}(x)/dx$ is the distribution of the total number of hits in the control pad in horizontal beam position. The number of hits in the control pad depends on x beam position, but not on the y position due to the location of the pad in the horizontal plane. For the dN_{cntr}/dx distribution we also use the experimental data from the silicon strip detector in the beam. We denote by $\tilde{n}^*$ the mean multiplicity in the ith bin under the condition of

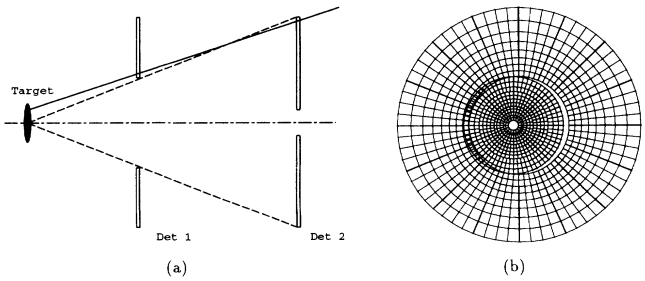

FIG. 18. (a) Plan view of the detectors, showing how an off-axis particle can hit both detectors. (b) Overlapping of the detectors from the interaction point as seen by an off-axis beam particle.

a hit in the control pad. It depends on the probability $w_i(x,y)$ that the same particle hits both the control pad and ith pad.

$$\tilde{n}_i^* = w_i(x,y)\frac{\tilde{n}_{\rm cntr}}{n_{\rm cntr}} + \left(1 - \frac{S_i}{S_{\rm cntr}} w_i(x,y)\right)\tilde{n}_i. \quad \text{(A7)}$$

Here $\tilde{n}_i$ and $\tilde{n}_{cntr}$ are mean multiplicities in the i-th and control pads, $w_i(x,y)$ is calculated as the fraction of the control pad area in common with the ith pad at offset (x,y). S_i and $S_{\rm cntr}$ are the areas of the control pad and ith pad.

In the above formulas we assume a Poisson multiplicity distribution in each pad. In this case the mean pad occupancy n_i and the mean pad multiplicity $\tilde{n}_i$ are related by the equality

$$n_i = 1 - \exp(-\tilde{n}_i). \quad \text{(A8)}$$

The results of the fit are presented in Fig. 19, where we show unbiased distributions in the pads, the distributions under the condition of a hit in the control pad, and the estimated distribution using the assumed vertical beam position distribution.

The fit ($\chi^2 = 9.8$ for 9 degrees of freedom) gives for the width the value $\sigma_y = 1.25 \pm 0.05$ mm, and in accordance with previous results [16] it shows that the beam is well centered at the center $y_0 = 0.01 \pm 0.04$ mm. Note that the accuracy in the parameters is more than adequate for the corrections we need (see results below).

The fitting procedure we used can be also generalized to extract the horizontal beam position distribution (which is independently measured by the silicon strip detector). We use this procedure to check the method. The result we find for the parameters of horizontal distribution ($\sigma_x = 1.26 \pm 0.2$ mm, $x_0 = 3.65 \pm 0.09$ mm) are in very good agreement with that measured by the beam vertex detector ($\sigma_x = 1.24 \pm 0.01$ mm, $x_0 = 3.50 \pm 0.01$ mm).

To illustrate the order of magnitude of the correction coefficients K_{ik} we present Fig. 20, where the correction coefficients for azimuthal and pseudorapidity correlation are shown. One should compare the figure with the final correlation results presented in the next chapter. The difference of K_{ik} from unity is approximately the correction value to the correlation function R_{ik}. One can see, that the corrections to the azimuthal correlations are significant, the correction to the pseudorapidity correlation are rather small for the correlation within small ϕ sectors and totally negligible to the pseudorapidity correlation in the full azimuthal angle space $\delta\phi = 2\pi$.

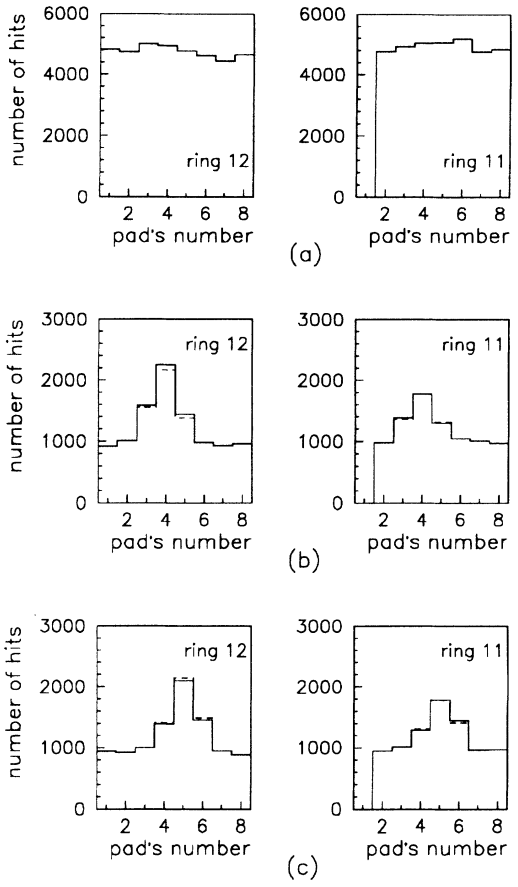

FIG. 19. (a) Unbiased hit distributions in the pads under study. (b) The distributions under the condition of hit in the control pad located right below the horizontal plane. The estimated distribution shown by dashed lines. (c) The same as (b) for the control pad located immediately above the horizontal plane.

APPENDIX B: SIMPLE CLUSTER MODEL

The main features of the cluster model can be explained in the following way. Let us assume that in some rapidity window we select the events with N_d directly produced charged particles and $N_r = \alpha N_d$ resonances which decay always to two charged particles. The total number of charged particles is $N = N_d + 2N_r = N_d(1 + 2\alpha)$. Under the assumption of no other correlations except the resonance decays we have a multinomial distribution for the number of particles in each rapidity bin with mean value proportional to the rapidity density.

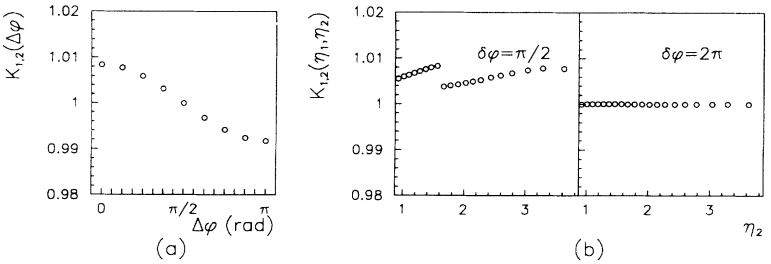

FIG. 20. (a) The correction coefficient for azimuthal angle correlation between sectors of size $\delta\phi = \pi/8$, within pseudorapidity window $0.96 < \eta < 1.61$. (b) The correction coefficient for pseudorapidity correlation for $\eta_1 = 2.15$, as a function of η_2 for two different sizes of azimuthal angle sectors $\delta\phi = \pi/2$ and 2π.

Using this distribution it is easy to derive the formula

$$C_2(y_1,y_2) \equiv \rho^{(2)}(y_1,y_2) - \rho(y_1)\rho(y_2) = R(y_1,y_2)\rho(y_1)\rho(y_2)$$
$$= 2\rho_r\left(\frac{y_1+y_2}{2}\right)w(y_1-y_2) - \frac{1}{N_d}\rho_d(y_1)\rho_d(y_2) - \frac{1}{N_r}\rho_s(y_1)\rho_s(y_2). \quad \text{(B1)}$$

Here $\rho_r(y)$ is resonance rapidity density, $\rho_d(y)$ is the rapidity density of directly produced particles, and $w(\Delta y)$ is the probability density to have rapidity separation Δy between products of the resonance decay, normalized to unity

$$\int_{-\infty}^{\infty} w(\Delta y)d\Delta y = 1. \quad \text{(B2)}$$

We denote by ρ_s the rapidity density of the secondaries from resonance decays,

$$\rho_s(y) = 4\int \rho_r(y_r)w[2(y-y_r)]dy_r. \quad \text{(B3)}$$

The resultant one particle density is $\rho(y) = \rho_d(y)+\rho_s(y)$. If the one-particle density does not significantly change over the range of the average rapidity separation between the products of the resonance decay we have

$$\rho_s(y) \approx 2\rho(y)_r \approx \alpha\rho_d(y). \quad \text{(B4)}$$

In this approximation

$$R(y_1,y_2) \approx \frac{\alpha}{1+\alpha}\rho^{-1}w(y_1-y_2) - \left(1+\frac{\alpha}{1+\alpha}\right)\frac{1}{N}. \quad \text{(B5)}$$

For isotropic decays the function $w(\Delta y/2) \propto \cosh^2(\Delta y)$ and with $(\Delta y)_{\max}$ depending on resonance and product masses, and for massless products can be very well fitted by a Gaussian with width $\approx$0.86. The contribution of other resonances (clusters) which can decay to more than two charged particles can be easily added. Taking into account also the nonzero width of our multiplicity windows, we find an expression (12) to which we fit our data. Parameter β in the formula (12) relates to the mean cluster decay multiplicity and for our simple model with only resonances decaying to two particles is

$$\beta = \frac{\alpha}{1+\alpha}. \quad \text{(B6)}$$

[1] J. Whitmore, Phys. Rep. **27**, 27 (1976).
[2] L. Foa, Phys. Rep. **22**, 2 (1975).
[3] F. Botterweck *et al.*, Z. Phys. C **51**, 37 (1991).
[4] R.E. Ansorge *et al.*, Z. Phys. C **37**, 191 (1988).
[5] T. Kafka *et al.*, Phys. Rev. D **16**, 1261 (1977).
[6] S.R. Amendolia *et al.*, Nuovo Cimento **31A**, 17 (1976).
[7] K. Eggert *et al.*, Nucl. Phys. **B86**, 201 (1975).
[8] W. Ko, Phys. Rev. Lett. **28**, 935 (1972).
[9] E.L. Berger, Nucl. Phys. **B85**, 61 (1975).
[10] *Intermittency in High Energy Collisions*, edited by F. Cooper, R. Hwa, and I. Sarcevic (World Scientific, Singapore, 1991).
[11] A. Bialas, Nucl. Phys. **A545**, 285 (1992).
[12] A. Bialas, Nucl. Phys. **A525**, 345 (1991).
[13] P. Carruthers, H.C. Eggers, and Ina Sarcevic, Nucl. Phys. **A545**, 285 (1992).
[14] J. Barrette *et al.*, Phys. Rev. C **46**, 312 (1992).
[15] J. Barrette *et al.*, Phys. Rev. Lett. **70**, 2996 (1993).
[16] K. Jayananda, Ph.D. thesis, University of Pittsburgh, 1991.
[17] M.I. Adamovich *et al.*, Phys. Lett. B **263**, 539 (1991).
[18] S. Voloshin and D. Seibert, Phys. Lett. B **249**, 321 (1990); D. Seibert and S. Voloshin, Phys. Rev. D **43**, 119 (1991).
[19] D. Seibert, Nucl. Phys. **A544**, 547c (1992); Phys. Rev. C **44**, 1223 (1991).
[20] KLM Collaboration, R. Holynski *et al.*, Phys. Rev. Lett. **62**, 733 (1989); Phys. Rev. C **40**, 2449 (1989).